CHEMISTRY OF MATERIALS
Cite This: Chem. Mater. 2018, 30, 8368−8374
Article
pubs.acs.org/cm

A Universal Method for the Preparation of Dual Network Reduced Graphene Oxide−Ceramic/Metal Foam Materials with Tunable Porosity and Improved Conductivity

Zhen Ge, Honghui Chen, Yuxin Ren, Peishuang Xiao, Yang Yang, Tengfei Zhang, Yanfeng Ma, and Yongsheng Chen*

The Centre of Nanoscale Science and Technology and Key Laboratory of Functional Polymer Materials, State Key Laboratory and Institute of Elemento-Organic Chemistry, College of Chemistry, Nankai University, Tianjin 300071, China

Supporting Information

ABSTRACT: Inorganic porous materials have found a great many applications in fields such as filtration, catalysis, and so forth. However, most of these materials have been prepared using complicated template and foaming methods and furthermore in many cases suffer from low electrical and thermal conductivity. Herein, we developed a universal and simple method for the synthesis of dual network reduced graphene oxide−ceramic/metal foam materials from commercial powders directly with graphene oxide as a 2D dispersant following a two-step process (solvothermal and partial sintering). This approach leads to the formation of a three-dimensional and interpenetrating dual network of both reduced graphene oxide and inorganic material. Importantly, this method not only is rather scalable but can also be applied universally for various ceramic materials, such as Al_2O_3 and TiO_2, and even metals such as Al and Cu. Furthermore, the material's porosity can be controlled by varying sintering temperatures and using different sizes of starting materials, ranging from several nanometers to a dozen micrometers. Because of the dual network architecture of both reduced graphene oxide and inorganic components, these materials exhibit multiple functions such as high porosity, improved electrical conductivity, and so forth. These results thus offer a general platform from various commercial inorganic powder materials directly for preparing porous but mechanically stable bulk materials, which are in high demand for catalysis, filtration, conductive ceramic, and porous electrode materials.

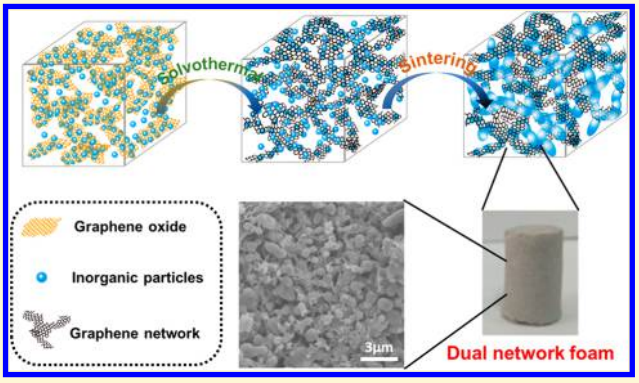

INTRODUCTION

Porous materials have been used for a wide variety of applications ranging from electrodes, catalyst support, absorption, and artificial skeletons to low-density structural materials.[1−4] Thus, tremendous efforts have been devoted to the preparation of porous materials with controlled structure and functions. Currently, most of the processes can be divided into four types, including (i) partial sintering, (ii) direct foaming, (iii) replica templates, and (iv) sacrificial fugitives.[5,6] Recently, blow-spinning,[7] freeze-drying,[8] and three-dimensional (3D) printing techniques[9] have also been developed. In the fabrication process of such porous materials, sacrificial components including foaming agents, template, and pore formers are necessary in most cases and need to be removed during or after sintering, leading to waste and pollution. Partial sintering is a conventional approach for the fabrication of porous ceramic and metal materials[10] without any sacrificial agent. Nevertheless, the materials produced with this approach often have low porosity, and low conductivity in the case of ceramic substrates, limiting its applications in catalysis or electronic devices.

Graphene sheets possess extraordinary conductivity, flexibility, and strength and have previously been used to prepare various composites with SiO_2,[11] Al_2O_3,[12] copper,[13] gold,[14] and other inorganic materials for the applications in catalysis, supercapacitors, lithium-ion batteries, and other fields.[15−21] But in these works, most of the aforementioned bulk composite materials are powders with randomly dispersed and individually isolated graphene sheets, so the excellent characteristics of graphene cannot be utilized completely. If graphene could be used to form a 3D and cross-linked framework, the obtained bulk material could exhibit the multiple functions derived from graphene, such as improved electronic conductivity. 3D graphene network materials have been prepared by template or assembly[22−25] in recent years. Previously, we have developed a method for the preparation of 3D chemical cross-linked graphene sponges showing superelasticity[26] using a simple solvothermal process[27] and found

Received: September 25, 2018
Revised: October 31, 2018
Published: November 1, 2018

DOI: 10.1021/acs.chemmater.8b04081
Chem. Mater. 2018, 30, 8368−8374

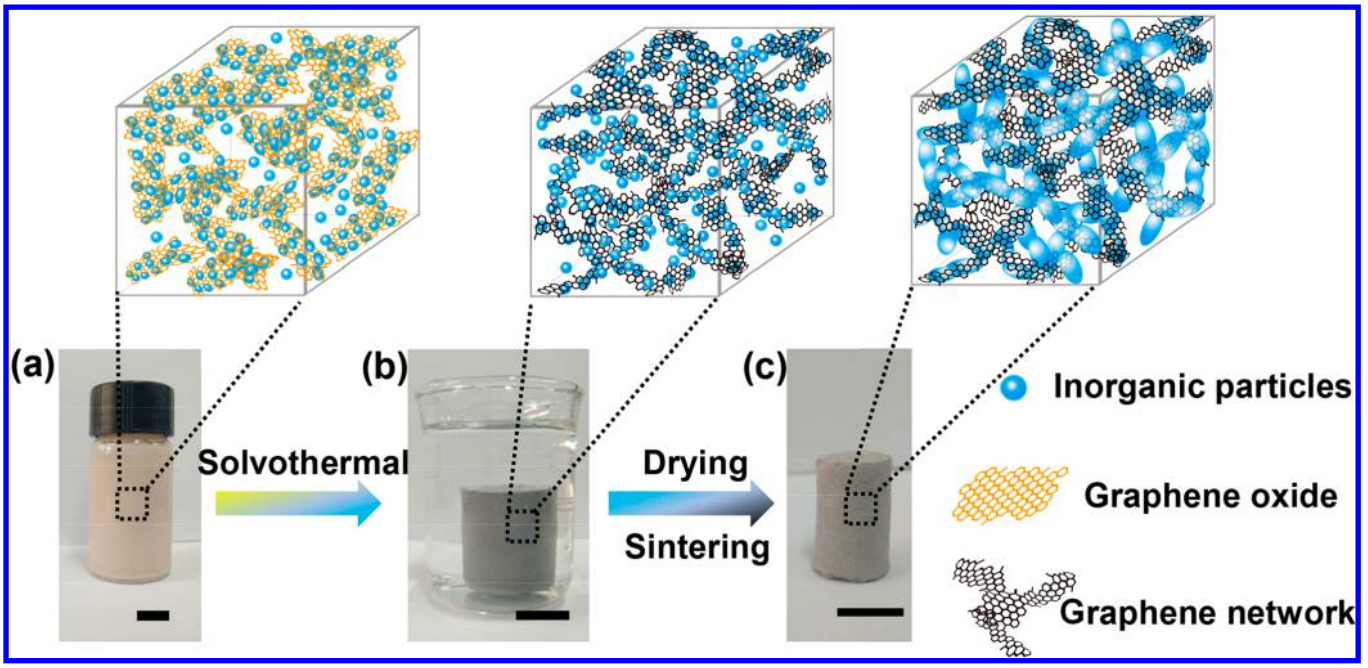

Figure 1. Illustration of the preparation of dual network reduced graphene oxide−inorganic foam materials: alumina as an example. (a) Photograph of Al_2O_3 particles dispersed in GO (1 mg mL^{-1}, 1 wt %) aqueous solution. (b) Columnar composite of 3DG network wrapping Al_2O_3 particles after the solvothermal process. (c) The foam composite with dual network of rGO and Al_2O_3 after drying and sintering. The scale bars are 1 cm.

possible applications in microwave absorption,[28] oil/water separation,[29] and water desalination.[30] Applying this idea to ceramic/metal materials, we propose a simple and scalable strategy combining a solvothermal approach and partial sintering for the preparation of dual network graphene−inorganic foam materials (DNGIF) with tunable porosity and other properties in the present work. In this dual network foam material, the inorganic network acts as a skeleton to strengthen the structure, and the reduced graphene oxide (rGO) network confines inorganic particles and offers the composite multiple functions, such as structural integrity and stability, and increased electrical conductivity for ceramic skeleton. Most importantly, for the first time, our approach offers a universal but simple powder metallurgy method which could be applied for various metals, such as aluminum, copper, and ceramic particles such as Al_2O_3 and TiO_2, with grain size widely tunable ranging from several nanometers to a dozen micrometers.

RESULTS AND DISCUSSION

Figure 1 illustrates the typical fabrication process. In brief, commercial inorganic particles without any treatment were used directly and dispersed in a solution of graphene oxide as a 2D dispersant. After solvothermal treatment, the 3D cross-linked rGO network was obtained, and it wrapped and confined particles like a cage leading to a stable and homogeneous bulk structure. The final product DNGIF was obtained by drying and sintering at a temperature lower than the melting point of inorganic materials applied.

For the fabrication of DNGIF, one of the prerequisites is to obtain a homogeneous dispersion of these ceramic/metal particles. It has been previously reported that the amphiphilic character of graphene oxide (GO) allows it to function as a two-dimensional surfactant to create organic solvent droplets stable in water.[31] Furthermore, carbon nanotubes and polyaniline powders[32] can also be dispersed well by GO. In this work, we found that metal, metal oxide, and ceramic powders could also be dispersed homogeneously in GO solution. More surprisingly, a stable dispersion could be obtained with a rather low GO content (<1 wt % of all the solid components) for various inorganic materials with various grain sizes, especially for the micrometer-sized powders. For example, Figure S1a demonstrates the stability of Al_2O_3 (particle size 200 nm in average diameter) dispersion in water with only 1 wt % GO after 24 h standing compared with the rather low stability of the dispersion without GO. For metal materials, taking copper powders as an example, similar behavior was also observed (Figure S2). The stability of the dispersion with GO may come from the strong interaction of GO sheets with the inorganic particles due to amphipathic characteristic caused by functional groups of OH/COOH and aromatic rings in GO sheets.[33] These multifunctional interactions may also cause the wrapping and confinement of the inorganic particles by GO sheets to prevent aggregation, as shown in Figure S1b,c. And for this method, large lamellar GO sheets (with average diameter of about 10 μm, but including some sheets over 30 μm, as shown in Figure S3) were chosen to stabilize nanometer- and micrometer-sized powders.

After obtaining a homogeneous dispersion, we prepared DNGIF materials via the solvothermal self-assembly procedure and sintering (details in the Experimental Section and Supporting Information). There are many OH, COOH, and epoxy groups located on GO sheets, and during the solvothermal treatment, superheated H_2O promotes acid-catalyzed reaction of those organic functional groups because of high H^+ concentration. These functional groups are expected to covalently interconnect the sheets, thereby forming 3D reduced graphene oxide (3DG) network.[27,34] At the same time, the inorganic particles absorbed and anchored on the rGO sheets in the 3DG network. After completely removing the solvent by air drying, the interaction between particles increases due to the capillary force[35] in the architecture, like the formation of a sandcastle.[36] Then the

DOI: 10.1021/acs.chemmater.8b04081
Chem. Mater. 2018, 30, 8368−8374

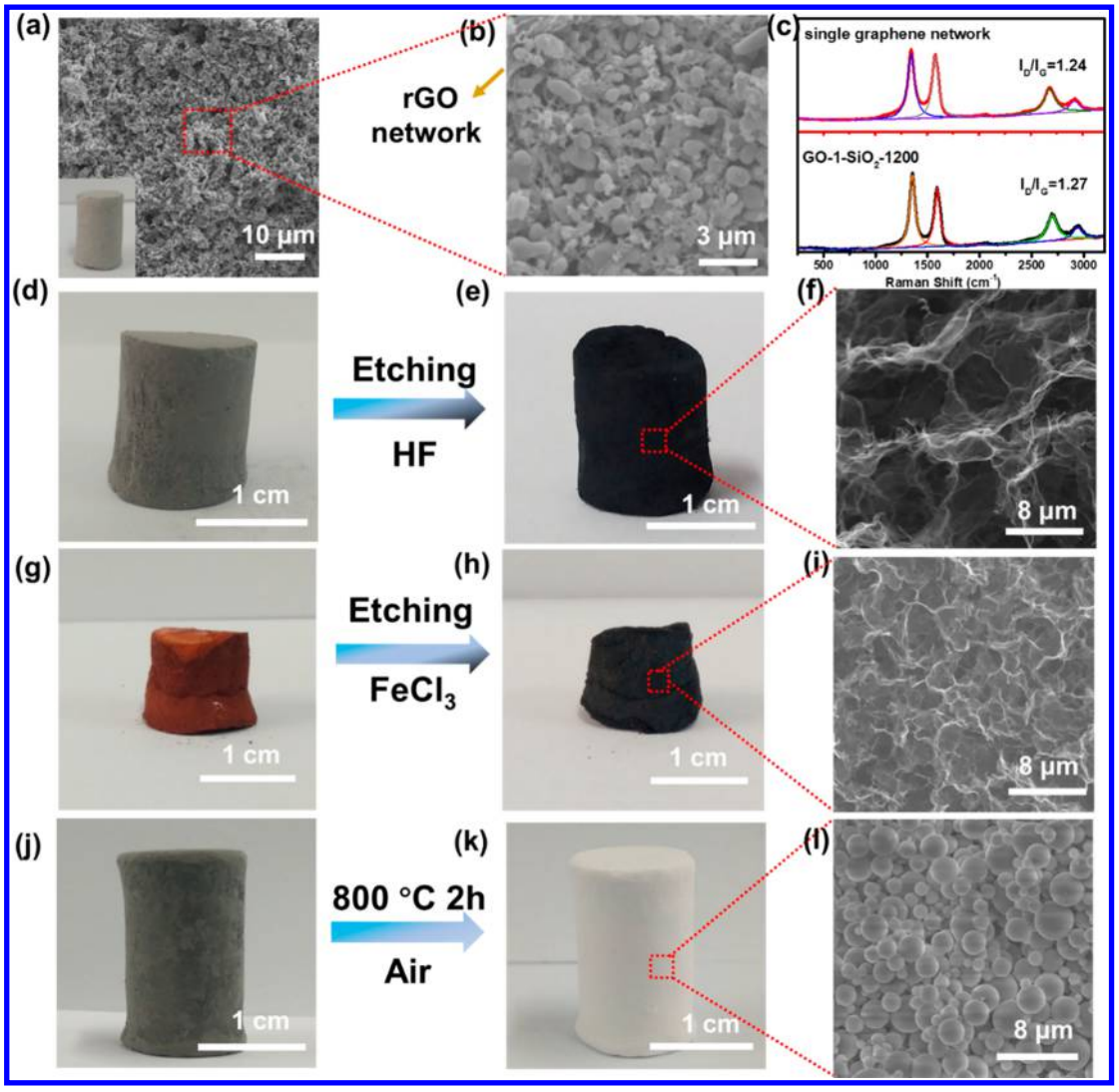

Figure 2. (a, b) SEM images of GO-1-Al_2O_3-1300 indicating the dual network of rGO and aluminia. (c) Raman spectra of the single graphene network and the sample GO-1-SiO_2-1200 indicating there is no observed difference for the 3DG network after removing the inorganic components. GO-1-SiO_2-1200 (d) is etched by hydrofluoric acid solution to get three-dimensional intercrossed graphene network (e). (f) SEM images of residual three-dimensional graphene network after etching. The sample GO-2-Cu-800 (g) is etched by $FeCl_3$ aqueous solution to get three-dimensional intercrossed graphene network (h). (i) SEM images of three-dimensional graphene network left after etching. Another sample GO-1-SiO_2-1200 (j) is annealed at 800 °C for 2 h in air to get inorganic network (k). (l) SEM images of SiO_2 network left after annealing in air.

free-standing porous green body was produced with volume shrinkage. Finally, partial sintering was carried out to strengthen the inorganic network and further reduce graphene oxide, leading to the formation of DNGIF materials. For example, GO-1-Al_2O_3-1300 (original graphene oxide is 1 wt % of the total solid content and sintered at 1300 °C for 4 h in argon forming Al_2O_3-based DNGIF) with high porosity (65%) was obtained, and a clear Al_2O_3-rGO dual network structure could be observed as shown by the scanning electron microscopic (SEM) images in Figure 2a,b.

The dual framework structure of DNGIF materials is further proved by removing the inorganic or rGO single network. Figure 2d shows the optical photograph of GO-1-SiO_2-1200 prepared in the same way (Supporting Information). After being etched in hydrofluoric acid solution (10%) for 5 days to remove SiO_2 completely, followed by a freeze-drying process, a free-standing bulk graphene sponge was left as shown in Figure 2e. The SEM image demonstrated that graphene sheets existed as 3D cross-linked network with micrometer-sized porous channels in the matrix (Figure 2f), and the XRD spectrum of left graphene network shows that there is only a broad peak at about 24°, indicating relatively poorer ordering of graphene sheets compared with that (Figure S4) of GO directly but similar as that of 3DG prepared directly from GO without other components.[28] For metal-based DNGIF materials, a similar graphene sponge with structural integrity was left after etching a GO-2-Cu-800 sample in $FeCl_3$ aqueous solution as shown in Figure 3g–i. Importantly, there is no observed difference for the 3DG network after removing the inorganic components as demonstrated in Raman spectra (Figure 2c). Also, the inorganic component network could also be kept after removing the graphene by annealing in air. For example, after annealing GO-1-SiO_2-1200 sample at 800 °C for 2 h in air, the entire SiO_2 network was still kept as shown in Figure 2j–l without any difference compared with the product GO-1-SiO_2-1200. The XRD spectrum of SiO_2 and the composite GO-1-SiO_2-1200 both show main peaks at 21.6°, indicating the crystal face (−4 0 4) of tridymite (PDF #18-1170, Figure S4).

DOI: 10.1021/acs.chemmater.8b04081
Chem. Mater. 2018, 30, 8368–8374

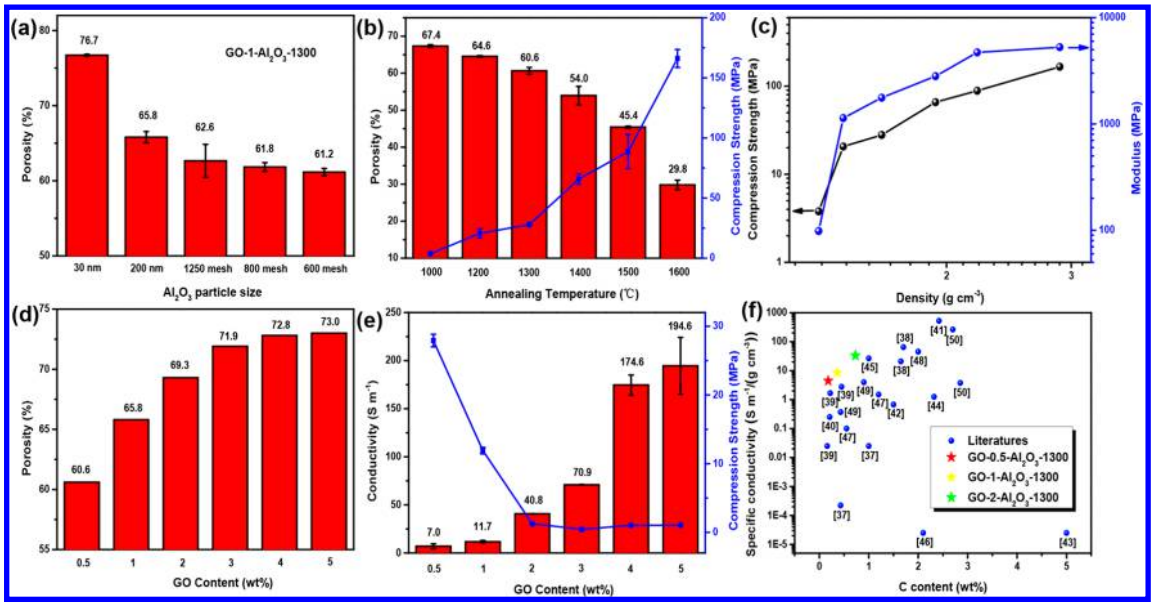

Figure 3. (a) Porosity of GO-1-Al_2O_3-1300 prepared from starting materials with different grain sizes. (b) Compression strength and porosity of GO-0.5-Al_2O_3 sintered at different temperatures from 1000 to 1600 °C. (c) Compression strength and modulus vs density of GO-0.5-Al_2O_3 sintered at different temperatures from 1000 to 1600 °C. (d) Porosity of Al_2O_3-based DNGIF with different original GO contents sintered at 1300 °C for 4 h. (e) Compression strength and conductivity of Al_2O_3-based DNGIF with different original GO content sintered at 1300 °C for 4 h. (f) A comparison of the specific conductivity and enhancer C content for this work and the literature data.

These results indicate that a dual network of both rGO and inorganic materials exists in the products.

In addition, the porosity of DNGIF materials can be tuned by varying the size of the starting materials, sintering temperature, and GO content. Commercial alumina powders with the grain size of 3 nm, 200 nm, 1250 mesh, 800 mesh, and 600 mesh were utilized directly for the preparation of DNGIF materials (Figures S5 and S6). As shown in Figure 3a, the porosity of GO-1-Al_2O_3-1300 samples decreases with increased grain size of starting powders. Powders with larger grain size by nature have higher compactness, leading to lower porosity after sintering in the same temperature than small particles. The sintering temperature also can control the porosity of the composites. When the samples GO-0.5-Al_2O_3 were sintered at different temperatures ranging from 1000 to 1600 °C, the porosity could be tuned between 67.4% and 29.8% and the density increased from 1.3 to 2.9 g cm^{-3}. At the same time, the compression strength increased from 4 to 166 MPa and the modulus increased from 98 to 5273 MPa as the sintering temperature was elevated (Figure 3b,c). In addition, the grain size grows from 0.3 to 2.5 μm when raising the sintering temperature from 1200 to 1600 °C because of the intrinsic grain coarsening of alumina (Figure S7). Additionally, the structure of graphene sheets is repaired better with the increased temperature, as demonstrated by the decrease of the intensity ratio of Raman D to G bands (I_D/I_G) from 1.60 to 0.58 (Figure S8a). Moreover, different GO contents can also change the porosity of DNGIF materials. These results indicate that with increasing GO loading, the porosity of the products could be increased due to graphene sheets better wrapping on the inorganic particles to prevent the particles from sintering and coarsening, as shown in Figure 3d. Similar works for different grain sizes and temperatures can also be applied to other materials such as Cu, TiO_2, and so forth, and similar results are obtained (Tables S1 and S2).

3D cross-linked rGO networks endow inorganic matrixes more functions, such as improved electrical and thermal conductivity in ceramic base porous composites. Figure 3e shows the compression strength and conductivity of Al_2O_3-based DNGIF with different original GO loadings from 0.5 to 5 wt % sintered at 1300 °C. The generated 3DG in the products acts as an electrically conducting network, and the composites show orders of increased electrical conductivity in the range of 7.0 S m^{-1} for GO-0.5-Al_2O_3-1300 and 11.7 S m^{-1} for GO-1-Al_2O_3-1300 compared to the insulation nature (conductivity $<10^{-12}$ S m^{-1}) of the materials without graphene. As can be expected, a higher original graphene oxide content leads to higher conductivity in the Al_2O_3-based DNGIF, reaching to 194.6 S m^{-1} for GO-5-Al_2O_3-1300. While the density, compression strength, and modulus decrease when GO loading increases as expected, the porosity and conductivity of the products increase (Figure S9). Carbon materials have been widely used to increase the conductivity of ceramic matrix.[37−51] As shown in Figure 3f, we compared the specific conductivity and carbon content of Al_2O_3-based DNGIF in our work with related reported results of Al_2O_3 and carbon composites. The Al_2O_3-based DNGIF we prepared clearly has a higher specific conductivity in the same carbon content compared with previous works. In particular, the specific conductivity of the sample GO-0.5-Al_2O_3-1300 reaches to 4.46 S m^{-1}/(g cm^{-3}) with only 0.17 wt % carbon amount (carbon amount was confirmed from thermogravimetry analysis and elemental analysis, Figure S10 and Table S3). Unlike most of the composites where graphene or other carbon materials are randomly dispersed in the matrix, DNGIF's three-dimensional cross-linked rGO network is more efficient in utilizing graphene for bulk materials, which can make a dramatic increase of electrical conductivity for the ceramic matrix. Additionally, we observed about 16% increase in thermal conductivity for GO-1-Al_2O_3-1300 compared to the comparison sample without graphene (Figure S11).

DOI: 10.1021/acs.chemmater.8b04081
Chem. Mater. 2018, 30, 8368−8374

Table 1. Properties of Various DNGIF Materials

sample	porosity (%)	density (g cm^{-3})	compression strength (MPa)	conductivity (S m^{-1})	modulus (MPa)	specific modulus (10^9 m^2 s^{-2})
GO-1-Al_2O_3-1300	65.0	1.4	11.9	11.7	462.5	330.4
GO-1-TiO_2-1000	41.3	2.5	20.9	463.9	1034.6	412.8
GO-1-SiO_2-1200	34.8	1.4	8.4	39.0	591.2	422.3
GO-2-HA-1000	61.0	1.2	4.4	0.1	164.7	137.2
GO-2-Al-650	64.0	1.0	0.4	1.8×10^4	15.9	15.9
GO-2-Fe-900	58.7	3.2	2.1	4.4×10^4	82.8	25.9
GO-2-Cu-800	50.7	4.3	1.1	5.4×10^4	13.8	3.2

To identify the universality of this novel powder metallurgy method, we proceeded with further experiments using more ceramic powder materials, such as TiO_2 (particle size 40 nm), SiO_2 (2 μm), hydroxyapatite (HA, 30 nm), and metal powders, like Cu (0.45 μm), Fe (~2 μm), and Al (~1 μm) as the raw powders, and the fabrication process was similar as described above as shown in the Supporting Information. Furthermore, this method can be used in different solvent systems as needed because GO sheets can form stable suspension in various solvents, such as water and alcohol, while still maintaining excellent flexibility and strength to wrap and immobilize the inorganic particles. For ceramic powders, the most common and cheapest water was chosen in this work, but for metal powders like copper and aluminum, *N*,*N*-dimethylformamide (DMF) was chosen because of its aprotic property and its inactivity to metals. After solvothermal and sintering processes, different DNGIF materials were prepared successfully in a cylindrical shape with obvious inorganic−rGO dual network structure as illustrated in Figure S12. These DNGIF materials maintain high porosity with decent compression strength and modulus but dramatically increased conductivity for ceramic matrix as shown in Table 1. The BET surface area data of these DNGIF materials were reported in Figure S13 and Table S4, showing that the surface area of composites increased because of the existence of rGO for the submicro- and micropowders. Furthermore, XRD and X-ray photoelectron spectroscopy (Figures S8b and S14−S16) of the DNGIF materials at every fabrication stage indicate that the composition and homogeneity was kept in solvothermal and sintering process. The results showed that the inorganic materials were stable during the whole preparation procedure. In particular, active metals, like aluminum and iron particles, were not oxidized owing to the use of aprotic solvent and the coating of rGO. In addition, different raw powders of various grain size also could be used to fabricate DNGIF materials with different porosity and strength (Figure 3a and Table S1). In summary, the strategy we reported in this work is versatile for different inorganic particles, including metal and ceramic particles with various grain sizes from several nanometers to a dozen micrometers.

CONCLUSIONS

In conclusion, we have demonstrated a novel and simple fabrication strategy for the synthesis of dual network reduced graphene oxide−ceramic/metal foam materials from homogeneously dispersed powders in a graphene oxide solution. This offers a new method for powder metallurgy techniques, combining a solvothermal approach and partial sintering (Figure 4a). In these novel porous materials, the inorganic network strengthens the whole architecture, while the 3D cross-linked rGO network contributes the previously mentioned effects: (i) locking inorganic particles in place by forming cages around them, producing a definite shape during the solvothermal self-assembly process; (ii) ensuring porosity by preventing excessive compacting and grain coarsening during the partial sintering process; and (iii) endowing the inorganic materials with more functions, such as improved electrical and thermal conductivity in the ceramic-based composites with low carbon content (Figure 4b). The porosity, conductivity, and strength of DNGIF materials can also be tuned by controlling the GO content, sintering temperature, and grain size of the raw powders. Most importantly, this strategy is universal for not only ceramic powders, like Al_2O_3 and TiO_2, but also metal powders, like aluminum and iron, in a wide grain size ranging from several nanometers to a dozen micrometers. Thus, these DNGIF materials might be well suited for scalable fabrication and have potential application in catalyst, filtration, conductive ceramic, and porous electrode.

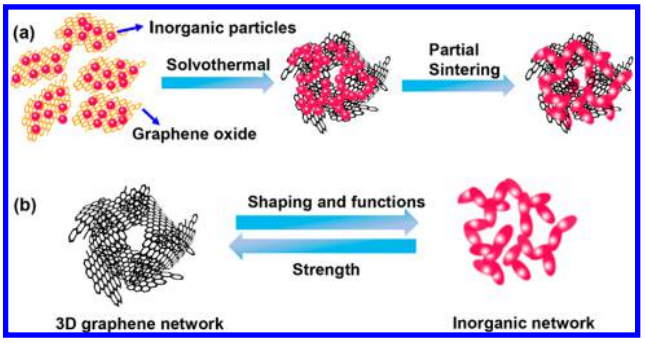

Figure 4. (a) Schematic diagram of the forming process of dual network rGO−inorganic foam materials. (b) The roles of single rGO network and inorganic network. 3DG network makes inorganic powders to form bulk materials and endows the composites functions while inorganic network strengthens the whole structure.

EXPERIMENTAL SECTION

Materials. Al_2O_3 particles (0.2 μm, Lot C10050432), TiO_2 particles (40 nm, Lot C10072686), SiO_2 powders (2 μm, Lot C10002052), hydroxyapatite (30 nm, Lot C10072145), and Cu powders (0.45 μm, Lot C10081930) were purchased from Macklin Reagent Co. Al powder (~1 μm, Lot D1811025) was purchased from Aladdin Reagent Co. Fe (~2 μm) were purchased from Xindun alloy Co. SEM images of these original inorganic powders were shown in Figure S17. All reagents were used as received without further purification and modification.

Synthesis of DNGIF. Graphene oxide (GO) was synthesized using a modified Hummers' method,[52] and the procedure is described in detail in the Supporting Information. In the precursor dispersion, the concentration of GO is from 1 to 2 mg mL^{-1} with the original GO content from 0.5 to 5 wt %. In this report, the concentration of GO is 1 mg mL^{-1} for ceramic particles, which is enough to obtain homogeneous dispersion. For some metal powders with higher densities, like copper and iron, we need to elevate the concentration of GO, and 2 mg mL^{-1} is appropriate in this work. The fabrication of GO-1-Al_2O_3-1300 as a typical example, 5.94 g of Al_2O_3 particles (0.2 μm, 99 wt %) was added into GO aqueous solution (1 mg mL^{-1}, 60

DOI: 10.1021/acs.chemmater.8b04081
Chem. Mater. 2018, 30, 8368−8374

mL, 1 wt %) in a beaker under strong agitation for 5 h. Then a little sulfuric acid (60 μL) was added for more stable dispersion. After that, the dispersion was poured into a Teflon-lined autoclave (100 mL) for a solvothermal process at 180 °C for 12 h. Then the porous product was transferred to a beaker and washed with water several times. After being dried at 60 °C for 24 h in air, the sample was annealed at 1300 °C for 4 h in an argon atmosphere to obtain GO-1-Al_2O_3-1300. For metal-based DNGIF, taking GO-2-Cu-800 as an example, 5.88 g of Cu particles (0.45 μm, 98 wt %) was added into GO DMF solution (2 mg mL^{-1}, 60 mL, 2 wt %) under strong agitation for 5 h. Then the dispersion was poured into a Teflon-lined autoclave (100 mL) for a solvothermal process at 180 °C for 12 h. After being dried at 60 °C for 36 h in air, the sample was annealed at 800 °C for 2 h in an argon atmosphere.

Characterizations. The compression strength of DNGIF materials (cut into 5 mm × 5 mm × 5 mm cube by diamond saw) was tested on an MTS CMT4204 universal testing machine at a loading rate of 0.5 mm min^{-1}. The electrical conductivity of DNGIF materials (cut into about ϕ 16 × 2 mm^2 cylinder by a diamond saw) was tested by the four-point probe method with a Keithley 2450 digital source meter, and three or four pieces of each sample were tested and average results reported. The thermal conductivity of samples (cut into ϕ 12.5 × 2.5 mm^2 cylinder by a diamond saw) was tested on a Netzsch LFA 457 laser thermal conducting instrument, and the average values were reported. The measurement of porosity was described in detail in the Supporting Information. XRD was carried out on a Rigaku Ultima IV X-ray diffractometer with Cu Kα radiation (λ = 0.15418 nm) at a scanning speed of 20 deg min^{-1}. Raman spectra were examined with a Renishaw inVia Raman spectrometer using laser excitation at 514.5 nm. SEM images were recorded using a Phenom Pro scanning electron microscope.

■ ASSOCIATED CONTENT

Supporting Information

The Supporting Information is available free of charge on the ACS Publications website at DOI: 10.1021/acs.chemmater.8b04081.

Detailed illustration of the fabrication process and test method, sedimentation tests, AFM, TG, XRD, and Raman of GO, photographs and SEM images of various alumina-based DNGIF materials, SEM images, Raman spectra, BET surface area, XPS spectra and XRD data of various ceramic/metal based DNGIF materials, thermogravimetry and thermal conductivity tests, porosity and compression strength of copper and TiO_2-based DNGIF materials, SEM images of original inorganic powders (PDF)

■ AUTHOR INFORMATION

Corresponding Author

*E-mail: yschen99@nankai.edu.cn.

ORCID

Yongsheng Chen: 0000-0003-1448-8177

Notes

The authors declare no competing financial interest.

■ ACKNOWLEDGMENTS

The authors gratefully acknowledge the financial support from Ministry of Science and Technology of China (MoST, 2016YFA0200200), the National Natural Science Foundation of China (NSFC, 21421001, 51633002, and 51472124), 111 Project (B12015), and Tianjin city (16ZXCLGX00100).

■ REFERENCES

(1) Porter, M. M.; Imperio, R.; Wen, M.; Meyers, M. A.; McKittrick, J. Bioinspired Scaffolds with Varying Pore Architectures and Mechanical Properties. *Adv. Funct. Mater.* **2014**, *24*, 1978−1987.

(2) Moene, R.; Makkee, M.; Moulijn, J. A. High Surface Area Silicon Carbide as Catalyst Support Characterization and Stability. *Appl. Catal., A* **1998**, *167*, 321−330.

(3) Yoon, B.-H.; Koh, Y.-H.; Park, C.-S.; Kim, H.-E. Generation of Large Pore Channels for Bone Tissue Engineering Using Camphene-Based Freeze Casting. *J. Am. Ceram. Soc.* **2007**, *90*, 1744−1752.

(4) Romero, A. R.; Elsayed, H.; Bernardo, E. Highly Porous Mullite Ceramics from Engineered Alkali Activated Suspensions. *J. Am. Ceram. Soc.* **2018**, *101*, 1036−1041.

(5) Jo, C.; Hwang, J.; Lim, W. G.; Lim, J.; Hur, K.; Lee, J. Multiscale Phase Separations for Hierarchically Ordered Macro/Mesostructured Metal Oxides. *Adv. Mater.* **2018**, *30*, 1703829.

(6) Kränzlin, N.; Niederberger, M. Controlled Fabrication of Porous Metals from the Nanometer to the Macroscopic Scale. *Mater. Horiz.* **2015**, *2*, 359−377.

(7) Wang, H.; Zhang, X.; Wang, N.; Li, Y.; Feng, X.; Huang, Y.; Zhao, C.; Liu, Z.; Fang, M.; Ou, G.; Gao, H.; Li, X.; Wu, H. Ultralight, Scalable, and High-Temperature-Resilient Ceramic Nanofiber Sponges. *Sci. Adv.* **2017**, *3*, e1603170.

(8) Fukushima, M.; Yoshizawa, Y.-I.; Ohji, T. Macroporous Ceramics by Gelation-Freezing Route Using Gelatin. *Adv. Eng. Mater.* **2014**, *16*, 607−620.

(9) Minas, C.; Carnelli, D.; Tervoort, E.; Studart, A. R. 3D Printing of Emulsions and Foams into Hierarchical Porous Ceramics. *Adv. Mater.* **2016**, *28*, 9993−9999.

(10) Ohji, T.; Fukushima, M. Macro-Porous Ceramics: Processing and Properties. *Int. Mater. Rev.* **2012**, *57*, 115−131.

(11) Kan, L.; Zheng, B.; Gao, C. Graphene-Templated Approach to Ultrathin Silica Nanosheets. *Chin. Sci. Bull.* **2012**, *57*, 3026−3029.

(12) Shahzadi, K.; Zhang, X.; Mohsin, I.; Ge, X.; Jiang, Y.; Peng, H.; Liu, H.; Li, H.; Mu, X. Reduced Graphene Oxide/Alumina, a Good Accelerant for Cellulose-Based Artificial Nacre with Excellent Mechanical, Barrier, and Conductive Properties. *ACS Nano* **2017**, *11*, 5717−5725.

(13) Liu, S.; Zhao, B.; Jiang, L.; Zhu, Y.-W.; Fu, X.-Z.; Sun, R.; Xu, J.-B.; Wong, C.-P. Core−Shell Cu@rGO Hybrids Filled in Epoxy Composites with High Thermal Conduction. *J. Mater. Chem. C* **2018**, *6*, 257−265.

(14) Hong, W.; Bai, H.; Xu, Y.; Yao, Z.; Gu, Z.; Shi, G. Preparation of Gold Nanoparticle/Graphene Composites with Controlled Weight Contents and Their Application in Biosensors. *J. Phys. Chem. C* **2010**, *114*, 1822−1826.

(15) Ambrosi, A.; Poh, H. L.; Wang, L.; Sofer, Z.; Pumera, M. Capacitance of p-and n-Doped Graphenes is Dominated by Structural Defects Regardless of the Dopant Type. *ChemSusChem* **2014**, *7*, 1102−1106.

(16) Buglione, L.; Chng, E. L. K.; Ambrosi, A.; Sofer, Z.; Pumera, M. Graphene Materials Preparation Methods Have Dramatic Influence Upon Their Capacitance. *Electrochem. Commun.* **2012**, *14*, 5−8.

(17) Ghosh, D.; Lim, J.; Narayan, R.; Kim, S. O. High Energy Density All Solid State Asymmetric Pseudocapacitors Based on Free Standing Reduced Graphene Oxide-Co_3O_4 Composite Aerogel Electrodes. *ACS Appl. Mater. Interfaces* **2016**, *8*, 22253−22260.

(18) Wang, Y.; Sofer, Z.; Luxa, J.; Chia, X.; Pumera, M. Graphene/Group 5 Transition Metal Dichalcogenide Composites for Electrochemical Applications. *Chem. - Eur. J.* **2017**, *23*, 10430−10437.

(19) Zoller, F.; Peters, K.; Zehetmaier, P. M.; Zeller, P.; Doeblinger, M.; Bein, T.; Sofer, Z.; Fattakhova-Rohlfing, D. Making Ultrafast High-Capacity Anodes for Lithium-Ion Batteries Via Antimony Doping of Nanosized Tin Oxide/Graphene Composites. *Adv. Funct. Mater.* **2018**, *28*, 1706529.

(20) Lu, Y.; Yang, Y.; Zhang, T.; Ge, Z.; Chang, H.; Xiao, P.; Xie, Y.; Hua, L.; Li, Q.; Li, H.; Ma, B.; Guan, N.; Ma, Y.; Chen, Y. Photoprompted Hot Electrons from Bulk Cross-Linked Graphene

DOI: 10.1021/acs.chemmater.8b04081
Chem. Mater. 2018, 30, 8368−8374

Materials and Their Efficient Catalysis for Atmospheric Ammonia Synthesis. *ACS Nano* **2016**, *10*, 10507−10515.
(21) Klimova, K.; Pumera, M.; Luxa, J.; Jankovsky, O.; Sedmidubsky, D.; Matejkova, S.; Sofer, Z. Graphene Oxide Sorption Capacity toward Elements over the Whole Periodic Table: A Comparative Study. *J. Phys. Chem. C* **2016**, *120*, 24203−24212.
(22) Cong, H.-P.; Ren, X.-C.; Wang, P.; Yu, S.-H. Macroscopic Multifunctional Graphene-Based Hydrogels and Aerogels by a Metal Ion Induced Self-Assembly Process. *ACS Nano* **2012**, *6*, 2693−2703.
(23) Chen, Z.; Ren, W.; Gao, L.; Liu, B.; Pei, S.; Cheng, H. M. Three-Dimensional Flexible and Conductive Interconnected Graphene Networks Grown by Chemical Vapour Deposition. *Nat. Mater.* **2011**, *10*, 424−428.
(24) Worsley, M. A.; Pauzauskie, P. J.; Olson, T. Y.; Biener, J.; Satcher, J. H., Jr.; Baumann, T. F. Synthesis of Graphene Aerogel with High Electrical Conductivity. *J. Am. Chem. Soc.* **2010**, *132*, 14067−14069.
(25) Xu, Y.; Sheng, K.; Li, C.; Shi, G. Self-Assembled Graphene Hydrogel Via a One-Step Hydrothermal Process. *ACS Nano* **2010**, *4*, 4324−4330.
(26) Zhang, T.; Chang, H.; Wu, Y.; Xiao, P.; Yi, N.; Lu, Y.; Ma, Y.; Huang, Y.; Zhao, K.; Yan, X.-Q.; Liu, Z.-B.; Tian, J.-G.; Chen, Y. Macroscopic and Direct Light Propulsion of Bulk Graphene Material. *Nat. Photonics* **2015**, *9*, 471−476.
(27) Wu, Y.; Yi, N.; Huang, L.; Zhang, T.; Fang, S.; Chang, H.; Li, N.; Oh, J.; Lee, J. A.; Kozlov, M.; Chipara, A. C.; Terrones, H.; Xiao, P.; Long, G.; Huang, Y.; Zhang, F.; Zhang, L.; Lepro, X.; Haines, C.; Lima, M. D.; et al. Three-Dimensionally Bonded Spongy Graphene Material with Super Compressive Elasticity and near-Zero Poisson's Ratio. *Nat. Commun.* **2015**, *6*, 6141.
(28) Zhang, Y.; Huang, Y.; Zhang, T.; Chang, H.; Xiao, P.; Chen, H.; Huang, Z.; Chen, Y. Broadband and Tunable High-Performance Microwave Absorption of an Ultralight and Highly Compressible Graphene Foam. *Adv. Mater.* **2015**, *27*, 2049−2053.
(29) Chang, H.; Qin, J.; Xiao, P.; Yang, Y.; Zhang, T.; Ma, Y.; Huang, Y.; Chen, Y. Highly Reversible and Recyclable Absorption under Both Hydrophobic and Hydrophilic Conditions Using a Reduced Bulk Graphene Oxide Material. *Adv. Mater.* **2016**, *28*, 3504−3509.
(30) Yang, Y.; Zhao, R. Q.; Zhang, T. F.; Zhao, K.; Xiao, P. S.; Ma, Y. F.; Ajayan, P. M.; Shi, G. Q.; Chen, Y. S. Graphene-Based Standalone Solar Energy Converter for Water Desalination and Purification. *ACS Nano* **2018**, *12*, 829−835.
(31) Kumar, H. V.; Huang, K. Y.; Ward, S. P.; Adamson, D. H. Altering and Investigating the Surfactant Properties of Graphene Oxide. *J. Colloid Interface Sci.* **2017**, *493*, 365−370.
(32) Kim, J.; Cote, L. J.; Kim, F.; Yuan, W.; Shull, K. R.; Huang, J. X. Graphene Oxide Sheets at Interfaces. *J. Am. Chem. Soc.* **2010**, *132*, 8180−8186.
(33) Bai, H.; Li, C.; Shi, G. Functional Composite Materials Based on Chemically Converted Graphene. *Adv. Mater.* **2011**, *23*, 1089−1115.
(34) Zhou, Y.; Bao, Q.; Tang, L. A. L.; Zhong, Y.; Loh, K. P. Hydrothermal Dehydration for the "Green" Reduction of Exfoliated Graphene Oxide to Graphene and Demonstration of Tunable Optical Limiting Properties. *Chem. Mater.* **2009**, *21*, 2950−2956.
(35) Roh, S.; Parekh, D. P.; Bharti, B.; Stoyanov, S. D.; Velev, O. D. 3D Printing by Multiphase Silicone/Water Capillary Inks. *Adv. Mater.* **2017**, *29*, 1701554.
(36) Koos, E.; Willenbacher, N. Capillary Forces in Suspension Rheology. *Science* **2011**, *331*, 897−900.
(37) Ahmad, K.; Pan, W.; Shi, S.-L. Electrical Conductivity and Dielectric Properties of Multiwalled Carbon Nanotube and Alumina Composites. *Appl. Phys. Lett.* **2006**, *89*, 133122.
(38) Benavente, R.; Pruna, A.; Borrell, A.; Salvador, M. D.; Pullini, D.; Peñaranda-Foix, F.; Busquets, D. Fast Route to Obtain Al_2O_3-Based Nanocomposites Employing Graphene Oxide: Synthesis and Sintering. *Mater. Res. Bull.* **2015**, *64*, 245−251.
(39) Centeno, A.; Rocha, V. G.; Alonso, B.; Fernández, A.; Gutierrez-Gonzalez, C. F.; Torrecillas, R.; Zurutuza, A. Graphene for Tough and Electroconductive Alumina Ceramics. *J. Eur. Ceram. Soc.* **2013**, *33*, 3201−3210.
(40) Fan, Y.; Jiang, W.; Kawasaki, A. Highly Conductive Few-Layer Graphene/Al_2O_3 Nanocomposites with Tunable Charge Carrier Type. *Adv. Funct. Mater.* **2012**, *22*, 3882−3889.
(41) Fan, Y.; Kang, L.; Zhou, W.; Jiang, W.; Wang, L.; Kawasaki, A. Control of Doping by Matrix in Few-Layer Graphene/Metal Oxide Composites with Highly Enhanced Electrical Conductivity. *Carbon* **2015**, *81*, 83−90.
(42) Fan, Y.; Wang, L.; Li, J.; Li, J.; Sun, S.; Chen, F.; Chen, L.; Jiang, W. Preparation and Electrical Properties of Graphene Nanosheet/Al_2O_3 Composites. *Carbon* **2010**, *48*, 1743−1749.
(43) Heo, Y.; Im, H.; Kim, J.; Kim, J. The Influence of $Al(OH)_3$-Coated Graphene Oxide on Improved Thermal Conductivity and Maintained Electrical Resistivity of Al_2O_3/Epoxy Composites. *J. Nanopart. Res.* **2012**, *14*, 1196.
(44) Inam, F.; Yan, H.; Reece, M. J.; Peijs, T. Dimethylformamide: An Effective Dispersant for Making Ceramic-Carbon Nanotube Composites. *Nanotechnology* **2008**, *19*, 195710.
(45) Ivanov, R.; Hussainova, I.; Aghayan, M.; Drozdova, M.; Pérez-Coll, D.; Rodríguez, M. A.; Rubio-Marcos, F. Graphene-Encapsulated Aluminium Oxide Nanofibers as a Novel Type of Nanofillers for Electroconductive Ceramics. *J. Eur. Ceram. Soc.* **2015**, *35*, 4017−4021.
(46) Jankovský, O.; Šimek, P.; Sedmidubský, D.; Huber, Š.; Pumera, M.; Sofer, Z. Towards Highly Electrically Conductive and Thermally Insulating Graphene Nanocomposites: Al_2O_3−Graphene. *RSC Adv.* **2014**, *4*, 7418−7424.
(47) Rul, S.; Lefèvre-Schlick, F.; Capria, E.; Laurent, C.; Peigney, A. Percolation of Single-Walled Carbon Nanotubes in Ceramic Matrix Nanocomposites. *Acta Mater.* **2004**, *52*, 1061−1067.
(48) Wang, K.; Wang, Y.; Fan, Z.; Yan, J.; Wei, T. Preparation of Graphene Nanosheet/Alumina Composites by Spark Plasma Sintering. *Mater. Res. Bull.* **2011**, *46*, 315−318.
(49) Yamamoto, G.; Omori, M.; Hashida, T.; Kimura, H. A Novel Structure for Carbon Nanotube Reinforced Alumina Composites with Improved Mechanical Properties. *Nanotechnology* **2008**, *19*, 315708.
(50) Zhan, G.-D.; Kuntz, J. D.; Garay, J. E.; Mukherjee, A. K. Electrical Properties of Nanoceramics Reinforced with Ropes of Single-Walled Carbon Nanotubes. *Appl. Phys. Lett.* **2003**, *83*, 1228−1230.
(51) Worsley, M. A.; Kucheyev, S. O.; Kuntz, J. D.; Olson, T. Y.; Han, T. Y.-J.; Hamza, A. V.; Satcher, J. H., Jr.; Baumann, T. F. Carbon Scaffolds for Stiff and Highly Conductive Monolithic Oxide-Carbon Nanotube Composites. *Chem. Mater.* **2011**, *23*, 3054−3061.
(52) Zhang, L.; Liang, J.; Huang, Y.; Ma, Y.; Wang, Y.; Chen, Y. Size-Controlled Synthesis of Graphene Oxide Sheets on a Large Scale Using Chemical Exfoliation. *Carbon* **2009**, *47*, 3365−3368.

DOI: 10.1021/acs.chemmater.8b04081
Chem. Mater. 2018, 30, 8368−8374